ISSN 0915-633X

NATIONAL INSTITUTE FOR FUSION SCIENCE

Non-dissipative Kinetic Simulation and Analytical Solution of Three-mode Equations of Ion Temperature Gradient Instability

T.-H. Watanabe, H. Sugama and T. Sato

(Received - Oct. 29, 1999)

NIFS-619 Dec. 1999

RESEARCH REPORT
NIFS Series

NAGOYA, JAPAN

Non-dissipative kinetic simulation and analytical solution of three-mode equations of ion temperature gradient instability

T.-H Watanabe, H.Sugama, and T.Sato
National Institute for Fusion Science, Toki, Gifu, 509-5292, Japan
(August 19, 1999, submitted to *Physics of Plasmas*)

A non-dissipative drift kinetic simulation scheme which rigorously satisfies the time-reversibility, is applied to the three-mode coupling problem of the ion temperature gradient (ITG) instability. It is found from the simulation that the three-mode ITG system repeats growth and decay with a period which shows a logarithmic divergence for infinitesimal initial perturbations. Accordingly, time average of the mode amplitude vanishes, as the initial amplitude approaches to zero. An exact solution is analytically given for a class of initial conditions. An excellent agreement is confirmed between the analytical solution and numerical results. The results obtained here provide a useful reference for basic benchmarking of theories and simulations of the ITG modes.

I. INTRODUCTION

Understanding the anomalous heat transport mechanism in high-temperature plasmas has been a central subject in the magnetic confinement fusion studies. The ion temperature gradient (ITG) instability[1,2] is widely recognized as the candidates which cause the anomalous ion thermal transport in the core of tokamaks. Many first-principle simulations as well as theoretical predictions have been carried out on ITG turbulence transport. Among them, the gyroparticle[3–6] and gyrofluid[7–10] simulations have largely contributed to development of transport modeling in the last decade. However, they have a discrepancy in the ion thermal diffusivity by a factor of two or more[5,11]. Since the reason for the difference between the two methods has not been completely understood yet, simple nonlinear problems, of which reliable solutions with sufficient accuracy are established, are preferable for benchmark studies of the numerical schemes.

The three-mode coupling of the ITG mode[3], as well as the drift waves[12–14], which is represented by a reduced set of the drift kinetic equation in a two-dimensional slab geometry, has been used to explain qualitatively a nonlinear saturation mechanism in the gyroparticle simulation[3]. The three-mode system has also been examined in comparison of the gyroparticle and gyrofluid simulations[11] and in a test of a nonlinear kinetic fluid closure method[15]. In the pioneering work by Lee *et al.*[12], they derived a nonlinear dispersion relation of the three-mode drift waves. However, so far, no exact solution of the three-mode coupling equations has been obtained analytically, except for a steady state solution with the Maxwellian velocity distribution[14]. The three-mode ITG and drift wave systems have also been studied by means of Eulerian drift kinetic (Vlasov) simulations[12–15]. The Vlasov simulation results, however, seem to suffer from numerical dissipation, because a dissipative integrator such as the predictor-corrector is employed for the collisionless drift kinetic equation. Therefore, it will be meaningful to develop a non-dissipative Vlasov simulation method, and to find numerical and analytical solutions of the three-mode equations. Results of the present study give a useful reference for benchmarking of various simulations and theories which are employed to investigate more complicated systems.

The remainder of the present paper is organized as follows. Section II gives the numerical simulation results of the three-mode coupling of the ITG modes, where a newly developed drift kinetic simulation method is also briefly explained. In section III, we will analytically derive an exact solution for a certain class of initial conditions from the three-mode ITG equations. Comparisons of the numerical and theoretical results are presented in Secs.II and III. Finally, we summarize the results in section IV.

II. DRIFTKINETIC SIMULATIONS

A. Simulation scheme

A basic scheme of our drift kinetic simulation is briefly presented here. In the long wave-length limit ($k_\perp \rho_i \ll 1$) we consider the electrostatic drift kinetic equation in a slab geometry,

$$\frac{\partial f}{\partial t} + v\nabla_\parallel f + \boldsymbol{v}_{E\times B}\cdot\nabla f + \frac{q}{m}E_\parallel \frac{\partial f}{\partial v} = 0\ . \qquad (1)$$

where $\boldsymbol{v}_{E\times B} = \boldsymbol{E}\times\boldsymbol{B}/B^2$, and v is the parallel velocity. It is easily found that Eq.(1) is reversible in time. Avoiding the numerical noise inherent in the particle simulation, we employ an Eulerian scheme which keeps the time-reversibility. A discrete spectral representation in the phase space or discretization on numerical grids makes Eq.(1) a set of ordinary differential equations. In a vector form, it can be written as

$$\frac{d\boldsymbol{U}}{dt} = \boldsymbol{F}(\boldsymbol{U})\ . \qquad (2)$$

In order to keep the time-reversibility of Eq.(1), a numerical time-integration scheme of Eq.(2) should also be reversible in time. It is well known that the symplectic scheme often used for integration of a Hamiltonian system, preserving a symplectic 2-form exactly, is non-dissipative, namely, time-reversible[16,17]. One of the simplest example is the leap-frog integrator which is a standard scheme in particle simulations[18] where particle motions are given by the Newton-Lorentz equation (not by drift motion of the guiding center). To trace the $\boldsymbol{E} \times \boldsymbol{B}$ drift particle motion with the time-reversibility, however, one needs to use an implicit symplectic method. This is because the Hamiltonian, $H(x,y,z,v) = mv^2/2 + e\phi(x,y,z)$, for the drift motion is non-separable for perpendicular coordinates x and y which are a conjugate pair of the coordinates (where $dx/dt = -\partial\phi/\partial y$ and $dy/dt = \partial\phi/\partial x$), while it is separable for the another conjugate pair, that is, the parallel coordinate z and the parallel velocity v. One of the simplest implicit schemes is the implicit midpoint rule,

$$\boldsymbol{U}^{n+1} - \boldsymbol{U}^n = \Delta t \boldsymbol{F}\left([\boldsymbol{U}^{n+1} + \boldsymbol{U}^n]/2\right) \ , \tag{3}$$

where n means a time step. This scheme is apparently reversible in time. When Eq.(3) is applied to the Hamilton's equation in canonical coordinates, $\boldsymbol{U} = (\boldsymbol{q}, \boldsymbol{p})$, it leads to a canonical transform from $(\boldsymbol{q}^n, \boldsymbol{p}^n)$ to $(\boldsymbol{q}^{n+1}, \boldsymbol{p}^{n+1})$[19].

We have employed Eq.(3) to integrate the drift kinetic equation,

$$f^{n+1} - f^n = -\Delta t \left\{\bar{f}, \bar{H}\right\} \ , \tag{4}$$

where $\bar{f} = (f^{n+1} + f^n)/2$ and $\{,\}$ means the Poisson brackets. $\bar{H}$ depends on $\bar{f}$ through the electrostatic potential ϕ. Although Eq.(4) is not a symplectic transform of f generated by a particle Hamiltonian, it preserves the time-reversibility, namely, is non-dissipative. It is also noteworthy that Eq.(4), which can be solved by iteration, is regarded as a discretized form of $\partial\bar{f}/\partial t = -\{\bar{f}, \bar{H}\}$ with second-order accuracy in time (namely, a time-centered finite difference). Construction of a fourth-order scheme is straightforward by successive operations of Eq.(3)[20]. Derivatives in the phase space shown in Eq.(1) are calculated in each Fourier space.

B. Simulation settings

The non-dissipative simulation scheme given above is applied to the three-mode coupling system of the ITG modes in a two-dimensional shearless slab geometry. Here, we consider the same model as that used in comparison of the gyroparticle and the gyrofluid simulations[11] except for truncation of the distribution function and a $\pi/2$ phase difference in x (direction of density and temperature gradients). The same model was also used by Mattor and Parker for examining a nonlinear kinetic fluid closure[15]. A rectangular simulation box of $L_x \times L_y$ is set in x-y plane with a uniform external magnetic field perpendicular to x-axis. Neglecting the parallel nonlinearity and expanding density and temperature scale length, L_n and L_T, of an assumed Maxwellian background, the drift kinetic equation for ions leads to

$$\begin{aligned}\partial_t \tilde{f} + \Theta v \partial_y \tilde{f} - \left(\partial_y \phi \partial_x \tilde{f} - \partial_x \phi \partial_y \tilde{f}\right) \\ = -\partial_y \phi \left[1 + (v^2 - 1)\eta_i/2 + \Theta v\right] F_M(v) \ ,\end{aligned} \tag{5}$$

where $\tilde{f}$ denotes a perturbed distribution function normalized by $\tilde{f} = \tilde{f}' L_n v_{ti}/\rho_i n_0$. Prime means a dimensional quantity. v_{ti}, ρ_i, and n_0 are the ion thermal velocity, the ion gyro-radius, and the background plasma density. Θ is defined as $\Theta = \theta L_n/\rho_i$ where an inclination of the magnetic field $\theta \ll 1$ is assumed. Other quantities are normalized as $x = x'/\rho_i$, $y = y'/\rho_i$, $v = v'/v_{ti}$, $t = t' v_{ti}/L_n$, $\eta_i = L_n/L_T$, and $\phi = e\phi' L_n/T_i\rho_i$ with the elementary charge e and the background ion temperature T_i ($= m_i v_{ti}^2$; m_i means the ion mass). We have taken $T_i = T_e$ throughout this paper. We also assume the adiabatic electron response and the quasi-neutrality. Thus,

$$\int \tilde{f} dv = \phi \ . \tag{6}$$

We employ the periodic boundary conditions in both x and y directions. Then, $\tilde{f}$ and ϕ can be written as

$$\tilde{f}(x,y,v.t) = \sum_{m,n} \tilde{f}_{m,n}(v,t) e^{\imath(k_x x + k_y y)} \ , \tag{7}$$

$$\phi(x,y,t) = \sum_{m,n} \phi_{m,n}(t) e^{\imath(k_x x + k_y y)} \ , \tag{8}$$

where $k_x = 2\pi m/L_x$ and $k_y = 2\pi n/L_y$ for $m = 0, \pm 1, \pm 2, ...$ and $n = 0, \pm 1, \pm 2, ...$ For studying the three-mode coupling, we only keep $(m,n) = (\pm 1, \pm 1)$ and $(\pm 2, 0)$ modes with the following symmetry conditions of $\tilde{f}_{1,1} = \tilde{f}_{-1,1} = \tilde{f}^*_{1,-1} = \tilde{f}^*_{-1,-1}$ and $\tilde{f}_{2,0} = \tilde{f}^*_{-2,0}$. Starting with an initial condition of

$$\tilde{f}(x,y,v,t=0) = \varepsilon F_M(v) \cos(kx) \cos(ky) \tag{9}$$

for $L_x = L_y = 2\pi/k$, we numerically follow a time evolution of $\tilde{f}$.

The physical parameters used here are $k = k_x = k_y = 0.1$ and $\eta_i = 10$. We have carried out several runs for different Θ scanning from 0.25 to 3. Amplitude of the initial perturbation, ε, is also changed from 10^{-5} to 1. The box size of the simulation is $L_x = L_y = 20\pi$ with 32×32 grid points. Spatial derivatives in Eq.(5) are calculated in the Fourier space. The velocity space of $-5 \le v \le 5$ is discretized by 129 grid points. A time step is taken to be $\Delta t = 0.25$.

We have made convergence checks for the time step, the resolution in the velocity space, the maximum velocity, and the accuracy of integration scheme, all of which give the same results as shown below.

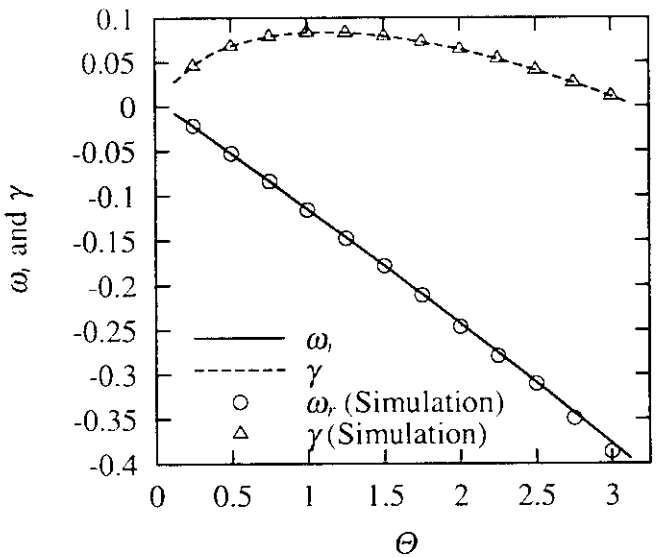

FIG. 1. Linear frequency (ω_r) and growth rate (γ) for different Θ obtained from simulations (marks) and linear analysis (lines) with $k = 0.1$ and $\eta_i = 10$.

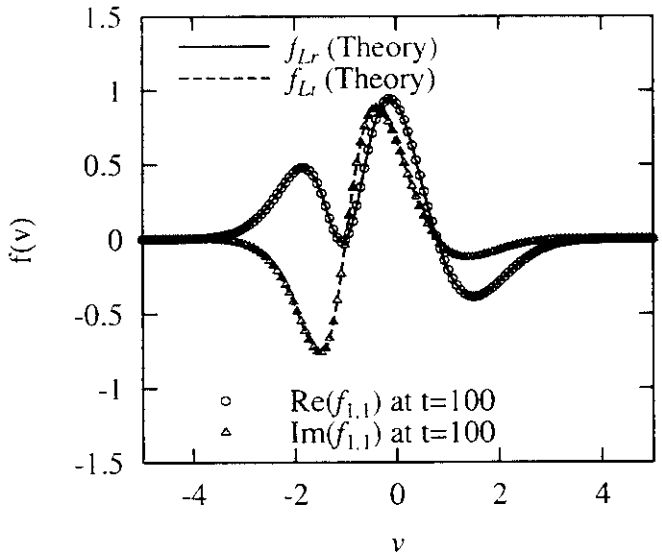

FIG. 2. Profiles of the distribution functions in the velocity space obtained from simulations (marks) for $\Theta = 1$ and $\varepsilon = 10^{-5}$ with $k = 0.1$ and $\eta_i = 10$ at $t = 100$. Solid and dashed lines indicate the linear eigenfunction.

C. Linear results

In Fig.1, the linear frequency ω_r and growth rate γ resulted from simulations for different Θ are shown by circular and triangular marks in comparison with the linear analysis. Simulation results shown here and in section II D are obtained by the second-order implicit scheme in Eq.(4). Solving the linear dispersion relation given in the next section (see Eq.(17)) numerically, we have calculated the theoretical values which agree with the simulation results. By the Nyquist criterion, we have also confirmed that only one eigenmode is unstable for a given value of Θ.

In Fig.2 plotted are profiles of $\tilde{f}_{1,1}$ for $\Theta = 1$ and $\varepsilon = 10^{-5}$ in the velocity space during the linear growth phase at $t = 100$. Here, a phase of $\tilde{f}_{1,1}$ is shifted in y so that $\phi_{1,1}$ is real. Amplitude of $\tilde{f}_{1,1}$ (and also $\tilde{f}_{2,0}$ in Fig.4) is normalized by $\phi_{1,1}$. Circular and triangular marks in Fig.2 show the simulation data on each grid point. Solid and dashed lines represent real and imaginary parts of a linear eigenfunction of the (1,1) mode, $f_{Lr}(v)$ and $f_{Li}(v)$, for the eigenfrequency $\omega_r + i\gamma$, which are defined in Eqs.(15) and (17) in section III. In the linear growth phase, $\tilde{f}_{1,1}$ is well fitted by the eigenfunction, while $\tilde{f}_{2,0}$ is negligible.

D. Nonlinear results

A time evolution of mode amplitudes for $\Theta = 1$ and $\varepsilon = 10^{-5}$ is shown in Fig.3, where the 0th-moment of $\tilde{f}_{1,1}$ and 2nd-moment of $\tilde{f}_{2,0}$ are represented by solid and dashed lines, respectively. After the initial linear growth phase, the amplitude of the $(1,1)$ mode is peaked at $t = 196$ due to appearance of the nonlinear $(2,0)$ mode.

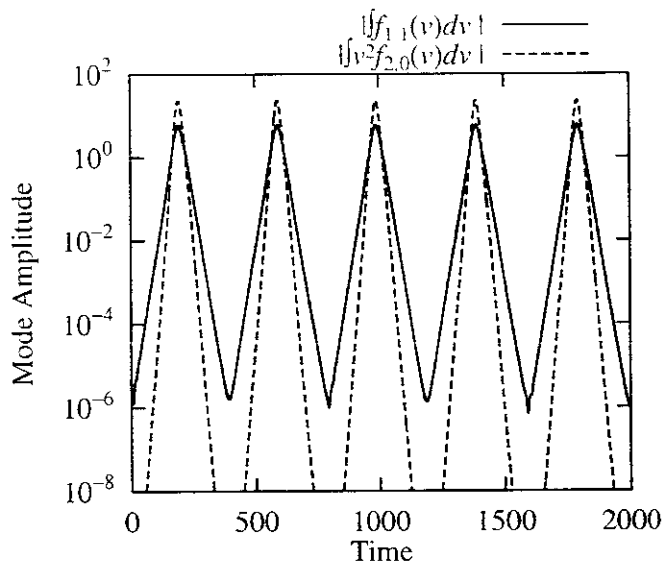

FIG. 3. Amplitude evolutions of 0th-moment of $(1,1)$ mode (solid) and 2nd-moment of $(2,0)$ mode (dashed) for $\Theta = 1$ and $\varepsilon = 10^{-5}$ with $k = 0.1$ and $\eta_i = 10$.

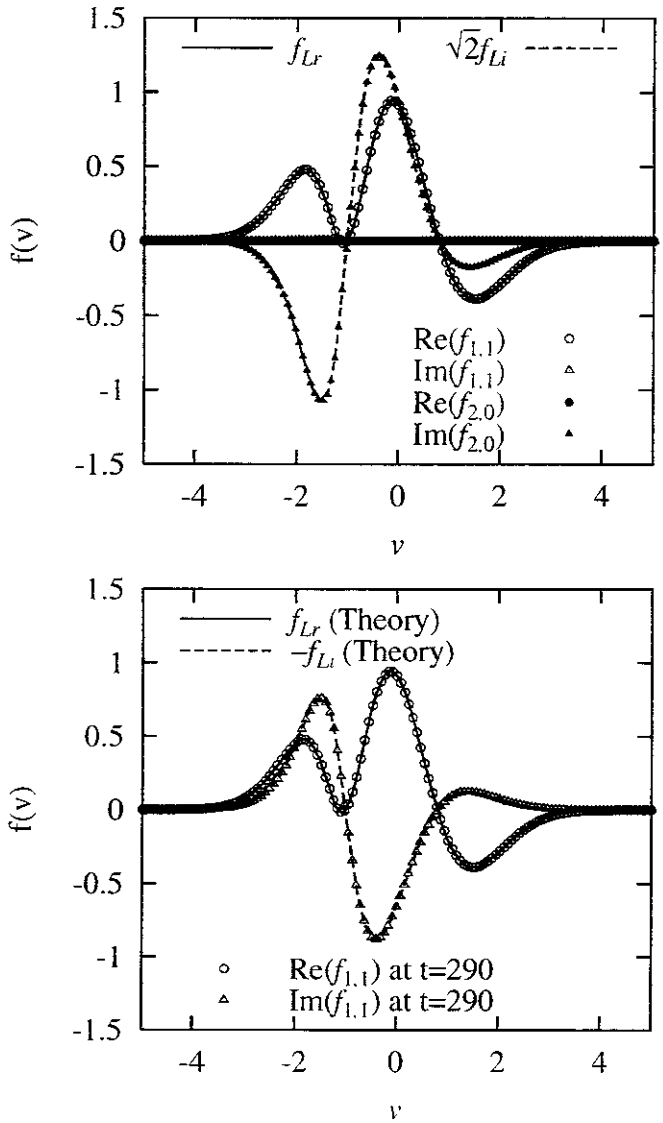

FIG 4. The same as FIG.2 but for $t = 196$ (upper) and $t = 290$ (lower).

Then, the $(1,1)$ mode exponentially decays with the same rate as the linear growth phase, and reaches to its minimum at $t = 393$. The minimum amplitude is nearly equal to the initial perturbation level. After that, the growth and decay are repeated with a regular oscillation period of $T = 394$.

Fig.4 shows profiles of $\tilde{f}_{1,1}$ and $\tilde{f}_{2,0}$ in the velocity space in the nonlinear phase. When the $(1,1)$ mode amplitude is peaked at $t = 196$, Im($\tilde{f}_{1,1}$) disappears (upper panel). On the other hand, one can see a finite amplitude of Im($\tilde{f}_{2,0}$), of which profile is scaled as $\sqrt{2}f_{Li}(v)$. During the decay phase, $\tilde{f}_{1,1}$ is fitted by the complex conjugate of $f_L(v)$. Neglecting small fluctuations of order ε, therefore, the linear and nonlinear evolutions of $\tilde{f}_{1,1}$ and $\tilde{f}_{2,0}$ are described in terms of f_{Lr} and f_{Li}. Being based on the simulation results, the three-mode ITG problem is fully explained by the analytical theory derived in the next section.

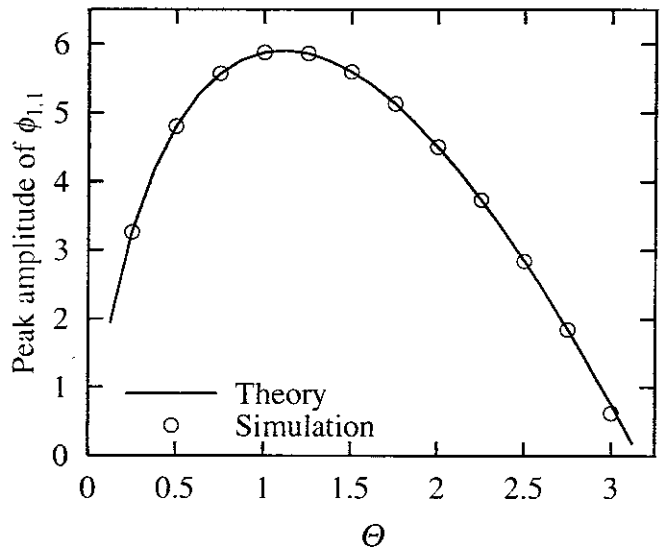

FIG. 5. Peak amplitudes of $\phi_{1,1}$ for different Θ (marks) with a theoretical prediction of $\gamma/\sqrt{2}k^2$ (solid) where $\varepsilon = 10^{-5}$ with $k = 0.1$ and $\eta_i = 10$.

The peak amplitude of $\phi_{1,1}$ provides a good benchmark for the simulation scheme, since the same test has been done by the gyroparticle and gyrofluid codes[11] as well as theoretical predictions[3,11]. A systematic scan for Θ from 0.25 to 3 has been made with $\varepsilon = 10^{-5}$. The peak levels are summarized in Fig.5 with a curve of $|\phi_{1,1}|_{\rm peak} = \gamma/\sqrt{2}k^2$ given by the theoretical prediction below. The simulation and the theory give the same peak level and scaling. The scaling of $|\phi_{1,1}|_{\rm peak} = \gamma/\sqrt{2}k^2$ agrees with previous theoretical works[3,11] except for a factor of $\sqrt{2}$.

As found in Fig.3, after the peaking, the mode amplitude decreases to the initial perturbation level. Thus, it is considered that the oscillation period T depends on ε. A similar nonlinear oscillation, but with different period and amplitude, was observed in a benchmark test of the nonlinear kinetic fluid closure[15] as well as the drift wave simulations[12–14]. In order to examine dependence of the oscillation period on the initial perturbation amplitude, we have performed six runs for $\Theta = 1$, changing ε as 10^{-5}, 10^{-4}, ... 1. The observed periods T in the simulations are plotted in Fig.6 versus the minimum amplitude $|\phi_{1,1}|_{\rm min}$, which shows a logarithmic dependence of T on $|\phi_{1,1}|_{\rm min}$. The analytical solution shown in the next section predicts the same period. The $|\phi_{1,1}|_{\rm min}$ dependence of T is easily explained by noting that a smaller initial perturbation stays longer time at the linear growing and decaying phases. Thus, a time average of $|\phi_{1,1}|$ approaches to zero as $\varepsilon \to 0$.

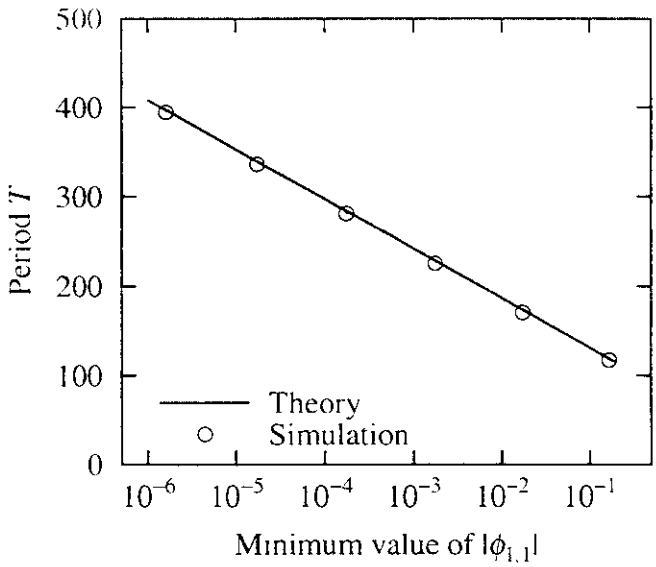

FIG. 6. Oscillation periods found in simulations for $\Theta = 1$ $k = 0.1$ and $\eta_i = 10$ depending on the initial perturbation level ε (where $\varepsilon = 10^{-5}, 10^{-4}, \ldots 1$) (marks) with a theoretical prediction given by Eq (36) (solid)

III. ANALYTICAL SOLUTIONS

A. Three-mode equations and linear solution

We derive exact nonlinear solutions of the three-mode problem of the ITG modes Hereafter, $\tilde{f}_{1,1}$, $\mathrm{Im}(\tilde{f}_{2,0})$ and $\phi_{1,1}$ are, respectively, denoted by f, h and ϕ for simplicity. From Eqs.(5) and (6) the three-mode ITG system is described by[3]

$$(\partial_t + ik\Theta v)f(v,t) + 2ik^2\phi(t)h(v,t) = -ik\phi(t)G(v) \ . \tag{10}$$

$$\partial_t h(v,t) = 4k^2\mathrm{Im}[\phi^*(t)f(v,t)] \ , \tag{11}$$

$$\phi(t) = \int dv\ f(v,t) \ . \tag{12}$$

where f and ϕ are complex-valued while h is real-valued. $G(v)$ is defined as

$$G(v) \equiv \left[1 + \frac{\eta_i}{2}(v^2 - 1) + \Theta v\right] F_M(v) \ . \tag{13}$$

We easily find

$$\partial_t \left[|f(v,t)|^2 + \frac{1}{2}h^2(v,t) + \frac{G(v)}{2k}h(v,t)\right] = 0 \ . \tag{14}$$

The linearized version of the three-mode equations has a linear solution of the form $[f(v,t), h(v,t), \phi(t)] = [f_L(v), h_L(v)\ \phi_L]\exp(-i\omega t)$ Here, the linear eigenfunctions are given by

$$\begin{aligned} f_L(v) &\equiv f_{Lr}(v) + if_{Li}(v) \\ &\equiv \frac{kG(v)}{(\omega_r - k\Theta v) + i\gamma} \\ &\equiv \frac{kG(v)[(\omega_r - k\Theta v) - i\gamma]}{(\omega_r - k\Theta v)^2 + \gamma^2} \ , \end{aligned} \tag{15}$$

$$h_L(v) \equiv 0, \quad \text{and} \quad \phi_L \equiv 1 \ \text{(normalization)} \ . \tag{16}$$

and the complex eigenfrequency $\omega = \omega_r + i\gamma$ is determined by the dispersion relation

$$\int dv\ f_L(v) \equiv \int dv \frac{kG(v)}{(\omega_r - k\Theta v) + i\gamma} = 1 \ , \tag{17}$$

where $\gamma > 0$ is assumed.

B. Nonlinear solution

Now, let us consider a certain class of exact solutions of the nonlinear three-mode ITG equations, which are written in terms of the real and imaginary parts of the eigenfunction $f_L(v)$ and the real eigenfrequency ω_r as

$$\begin{aligned} f(v,t) &= [a(t)f_{Lr}(v) + ib(t)f_{Li}(v)]\exp(-i\omega_r t), \\ h(v,t) &= c(t)f_{Li}(v) \\ \phi(t) &= a(t)\exp(-i\omega_r t) \ . \end{aligned} \tag{18}$$

where $a(t)$, $b(t)$, and $c(t)$ are real-valued functions of the time t. The linear solution given by Eqs.(15)-(17) corresponds to the case, in which $a(t) = b(t) \propto \exp(\gamma t)$ and $c(t) = 0$ Substituting these into Eqs.(10)-(12) and using Eq.(15), we obtain the ordinary differential equations for $[a(t), b(t), c(t)]$.

$$\begin{aligned} da/dt &= \gamma b \ . \\ db/dt &= \gamma a - 2k^2 ac \ , \\ dc/dt &= 4k^2 ab. \end{aligned} \tag{19}$$

These equations have two types of stationary solutions, which are written as

$$(a,b,c) = (0,0,c_s) \quad \text{and} \quad (a,b,c) = (a_s, 0, \gamma/2k^2), \tag{20}$$

respectively, where a_s and c_s are arbitrary constants. The former solution in Eq.(20) is c-axis, and the latter one is parallel to a-axis. From Eq.(19), we easily find

$$\frac{d}{dt}\left(c - \frac{2k^2}{\gamma}a^2\right) = 0 \ , \tag{21}$$

and

$$\frac{d}{dt}\left(b^2+\frac{1}{2}c^2-\frac{\gamma}{2k^2}c\right)=0\ . \tag{22}$$

Also, combining these two equations, we have

$$\frac{d}{dt}\left(a^2+b^2+\frac{1}{2}c^2-\frac{\gamma}{k^2}c\right)=0\ , \tag{23}$$

which corresponds to Eq.(14). Thus, as shown in Fig.7, the orbit of the solution in the (a,b,c)-phase space is given by the intersection between the two surfaces, which are written as

$$c-\frac{2k^2}{\gamma}a^2=C_1\ , \tag{24}$$

and

$$b^2+\frac{1}{2}c^2-\frac{\gamma}{2k^2}c=C_2\ , \tag{25}$$

where C_1 and C_2 are constants. The orbit is also on the spheroid surface,

$$a^2+b^2+\frac{1}{2}c^2-\frac{\gamma}{k^2}c=C_2-\frac{\gamma}{2k^2}C_1\ . \tag{26}$$

We also note that the stationary solutions $(a_s,0,\gamma/2k^2)$ with varying a_s form the central axis of the elliptic column given by Eq.(25), which is also shown in Fig.8. A simple estimate of the peak amplitude of $|\phi|_{\rm peak}=\gamma/\sqrt{2}k^2$ shown in Fig.5 is given as follows. Substitute $C_1=C_2=0$ to Eqs.(24) and (25) for infinitesimal initial perturbation. Since $da/dt=0$ at the peak of the mode amplitude, $b=0$ (see Eq.(19)). Then, one finds $a=\gamma/\sqrt{2}k^2$, $b=0$, and $c=\sqrt{2}a=\gamma/k^2$ which also gives the scaling of $\mathrm{Im}(\tilde{f}_{2.0})=\sqrt{2}f_{L_i}$ shown in Fig.4.

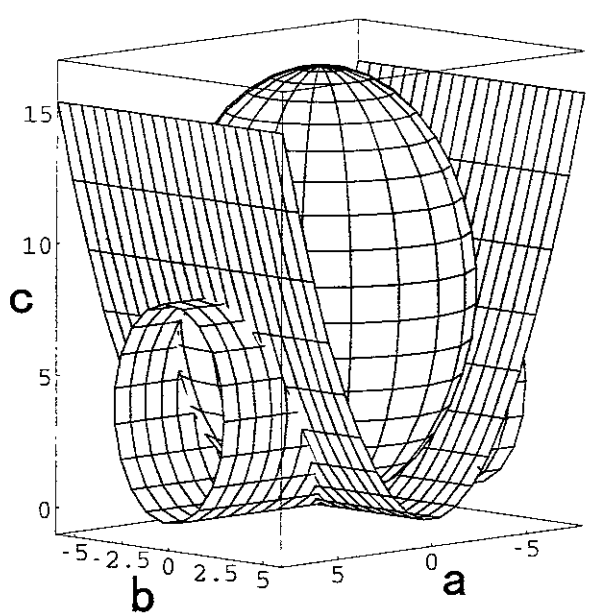

FIG. 7. An orbit of the exact solution for $\Theta=1$, $k=0.1$ and $\eta_i=10$ in the (a,b,c)-phase space shown by the intersection of parabolic and elliptic column surfaces which is also on a spheroid.

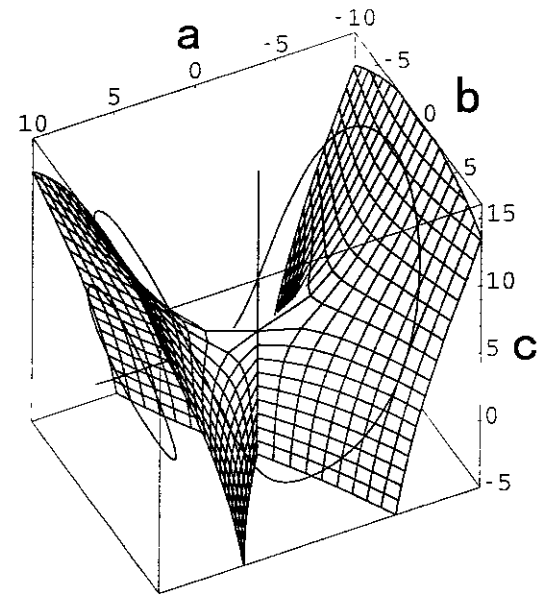

FIG. 8. A separatrix surface of $r=0$ for the same parameters as FIG.7 with stationary solutions of $(0,0,c_s)$ and $(a_s,0,\gamma/2k^2)$, where two solid curves represent typical solutions for $r>0$ and $r<0$.

Using Eqs.(24)–(26), the solution of Eq.(19) for the initial condition $(a,b,c)_{t=0}=(a_0,b_0,c_0)$ can be obtained by

$$b^2=b_0^2+\frac{\gamma}{2k^2}(c-c_0)-\frac{1}{2}(c^2-c_0^2)\ , \tag{27}$$

$$c=c_0+\frac{2k^2}{\gamma}(a^2-a_0^2), \tag{28}$$

and

$$a(t)=\begin{cases}\beta\,\mathrm{dn}\left[\mathrm{dn}^{-1}(a_0/\beta)-(\sqrt{\alpha}/\beta)\gamma t\right] & \text{for } r>0\\ \beta\,\mathrm{cn}\left[\mathrm{cn}^{-1}(a_0/\beta)-(\sqrt{\alpha}/\beta)\gamma t\right] & \text{for } r<0\ ,\end{cases} \tag{29}$$

where the Jacobi elliptic functions are defined by $\mathrm{dn}u=(1-\kappa^2\mathrm{sn}^2u)^{1/2}$, $\mathrm{cn}u=(1-\mathrm{sn}^2u)^{1/2}$, and $\int_0^{\mathrm{sn}u}[(1-x^2)(1-\kappa^2x^2)]^{-1/2}dx=u$. Here, the parameters α, β, and κ^2 are given by

$$\alpha=\begin{cases}\frac{p^2}{2q}-r+\sqrt{\frac{p^2}{2q}\left(\frac{p^2}{2q}-2r\right)} & \text{for } r>0\\ \frac{p^2}{2q}-2r+\sqrt{\frac{p^2}{2q}\left(\frac{p^2}{2q}-2r\right)} & \text{for } r<0\ ,\end{cases} \tag{30}$$

$$\beta=\begin{cases}\left(\frac{\alpha}{q}\right)^{1/4} & \text{for } r>0\\ \left(\frac{\alpha}{q}\kappa^2\right)^{1/4} & \text{for } r<0\ ,\end{cases} \tag{31}$$

and

$$\kappa^2 = 1 - \frac{|r|}{\alpha}. \tag{32}$$

respectively, where

$$p = 1 - \frac{2k^2}{\gamma}c_0 + \frac{4k^4}{\gamma^2}a_0^2 , \tag{33}$$

$$q = \frac{2k^4}{\gamma^2}, \tag{34}$$

$$r = a_0^2 - \frac{2k^2}{\gamma}a_0^2 c_0 + \frac{2k^4}{\gamma^2}a_0^4 - b_0^2 . \tag{35}$$

C. Orbit in (a,b,c)-phase space

The solutions given above are periodic functions of the time t. For $r > 0$, $a(t)$ takes any value in the range $\beta(r/\alpha)^{1/2} \le |a| \le \beta$, and its sign is a constant determined by the initial value a_0. On the other hand, for $r < 0$, the value range of $a(t)$ is given by $-\beta \le a \le \beta$ and the sign of a changes with time. Thus, the shape of the closed orbit in the (a, b, c)-phase space is like a butterfly for $r < 0$. The period T of the solution $[a(t), b(t), c(t)]$ is written as

$$T = \begin{cases} \frac{2\beta}{\sqrt{\alpha\gamma}}K(\kappa) & \text{for } r > 0 \\ \frac{4\beta}{\sqrt{\alpha\gamma}}K(\kappa) & \text{for } r < 0 , \end{cases} \tag{36}$$

where $K(\kappa)$ is the complete elliptic integral of the first kind. The period for $r > 0$ given by Eq.(36) agrees with the simulation results in Fig.6.

We find that, as $(a_0, b_0, c_0) \to (0, 0, 0)$, $r \to 0$ and

$$T \sim \begin{cases} \gamma^{-1}\log(1/|r|) & \text{for } r \to +0 \\ 2\gamma^{-1}\log(1/|r|) & \text{for } r \to -0 . \end{cases} \tag{37}$$

Thus, the period T shows the logarithmic divergence for $r \to 0$. The solution $[a(t), b(t), c(t)]$ stays most of the period in the neighborhood of the stationary point $(0, 0, 0)$. For the case of $r = 0$, the solution is no longer periodic (or $T = \infty$) and its orbit emerges from (approaches to) the stationary point $(0, 0, 0)$ for $t \to -\infty$ $(+\infty)$. The set of (a_0, b_0, c_0) satisfying $r = a_0^2 - \frac{2k^2}{\gamma}a_0^2 c_0 + \frac{2k^4}{\gamma^2}a_0^4 - b_0^2 = 0$ forms a separatrix surface, which separates the phase space into the two regions ($r > 0$ and $r < 0$; see Fig.8) which are filled with the two different types of orbits given by Eqs.(27)–(29).

Finally, Fig.9 shows the two kinds of orbits for $r > 0$ with $(a_0, b_0, c_0) = (0.25, 0, 0)$ (upper) and $r < 0$ with $(a_0, b_0, c_0) = (0, 0.25, 0)$ (lower) by solid lines.

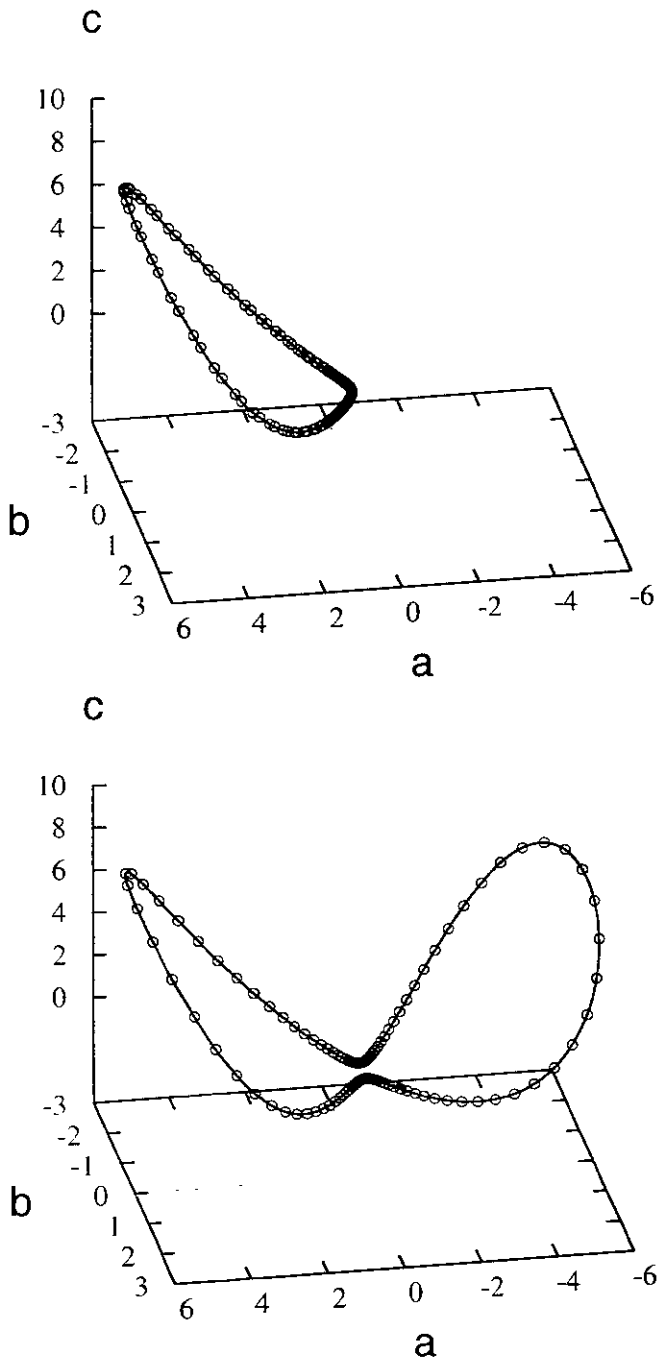

FIG 9 Typical two orbits of solutions for $r > 0$ (upper) and $r < 0$ (lower) followed by the Vlasov simulation results for the initial conditions given by Eq.(38) for the same parameters as FIG.7. The solid lines represent the analytical solutions. Circular marks show the simulation results at every $2L_n/v_{ti}$.

We also plot circular marks representing the Vlasov simulation results at every $2L_n/v_{ti}$ which are, respectively, started with initial conditions of

$$f(v, t = 0) = a_0 f_{Lr}(v) \text{ (upper)}$$

and $f(v, t=0) = b_0 f_{L_i}(v)$ (lower) . (38)

As shown in Fig.9, a perfect agreement is found between the analytical solutions and the Vlasov simulation results. It is clearly confirmed that our numerical scheme strictly preserves the time-reversibility, the periodicity, and the initial value dependence of the exact solution. Here, we have assumed the initial conditions in Eq.(38) which satisfy Eq.(18), while a different type of the initial condition has been employed for the simulations in the last section. Nevertheless, the simulation results in the last section are well described by the analytical solution. It is because, if the initial perturbation is sufficiently small, only one linearly unstable eigenmode in the form of Eq.(18) becomes dominant at early time stage. Thus, the amplitude oscillation found in Fig.3, where $a > 0$, is explained by the periodic motion along the orbit for $r > 0$ in the (a, b, c)-phase space.

IV. SUMMARY

We have developed a non-dissipative Eulerian kinetic simulation method which rigorously preserves the time-reversibility inherent in the collisionless drift kinetic equation. The simulation method is applied to the three-mode ITG problem. An analytical solution of the three-mode ITG equations is also derived here, and successfully describes the nonlinear evolution of the three-mode system. We have found an excellent agreement between the simulation results and the analytical solution.

The main results obtained here are summarized as follows: Amplitudes of $(\pm 1, \pm 1)$ and $(\pm 2, 0)$ modes repeat the nonlinear oscillation, and evolves in time along a closed orbit which encircles the stationary solution $(a_s, 0, \gamma/2k^2)$ in the phase space. This fact reflects the time-reversibility of Eq.(5). Thus, the three-mode system never reaches to a steady state, unless the initial condition coincides with the stationary solutions in Eq.(20). Since the solution stays most of the period in the neighborhood of the stationary point $(0, 0, 0)$ with the exponential time dependence, the oscillation period has a logarithmic dependence on the initial mode amplitude. Thus, the time average of the mode amplitude vanishes, as the infinitesimal initial perturbation approaches to zero.

The success of the present simulation, of which validity is confirmed by the theoretical analysis, is achieved by a proper choice of the numerical scheme with no dissipation. If the scheme is dissipative, it affects estimates of the oscillation period and the averaged amplitude. Application of the present numerical method to a multi-mode coupling system and the gyrokinetic equations is remained for future works.

ACKNOWLEDGMENTS

One of the authors (T.-H.W.) would like to thank Y.Todo for his fruitful comments and discussions. Numerical computations in this study are performed on the NIFS MISSION System (Man-Machine Interactive System for Simulation).

[1] L.I.Rudakov and R.Z.Sagdeev, Dokl.Akad.Nauk SSSR **138**, 581 (1961) [English transl.: Soviet Phys.Dokl. **6**, 415 (1961)].

[2] B.Coppi, M.N.Rosenbluth, and R.Z.Sagdeev, Phys.Fluids **10**, 582 (1967).

[3] W.W.Lee and W.M.Tang, Phys.Fluids **31**, 612 (1988).

[4] S.E.Parker, W.W.Lee, and R.A.Santoro, Phys.Rev.Lett. **71**, 2042 (1993).

[5] A.M.Dimits, T.J.Williams, J.A.Byers, and B.I.Cohen, Phys.Rev.Lett. **77**, 71 (1996).

[6] Z.Lin, T.S.Hahm, W.W.Lee, W.M.Tang, and R.B.White, Science **281**, 1835 (1998).

[7] W.Dorland and G.W.Hammett, Phys.Fluids B **5**, 812 (1993).

[8] R.E.Waltz, G.D.Kerbel and J.Milovich, Phys.Plasmas **1**, 2229 (1994).

[9] M.Kotschenreuther, W.Dorland, M.A.Beer, and G.W.Hammett, Phys.Plasmas **2**, 2381 (1995).

[10] M.A.Beer, G.W.Hammett, G.Rewoldt, E.J.Synakowski, M.C.Zarnstorff, and W.Dorland, Phys.Plasmas **4**, 1792 (1997).

[11] S.E.Parker, W.Dorland, R.A.Santoro, M.A.Beer, Q.P.Liu, W.W.Lee, and G.W.Hammett, Phys.Plasmas **1**, 1461 (1994).

[12] W.W.Lee, J.A.Krommes, C.R.Oberman, and R.A.Smith, Phys.Fluids **27**, 2652 (1984).

[13] J.F.Federici, W.W.Lee, and W.M.Tang, Phys.Fluids **30**, 425 (1987).

[14] A.M.Dimits, Phys.Fluids B **2**, 1768 (1990).

[15] N.Mattor and S.E.Parker, Phys.Rev.Lett. **79**, 3419 (1997).

[16] E.Forest and R.D.Ruth, Physica D **43**, 105 (1990).

[17] H.Yoshida, Phys.Lett. A **150**, 262 (1990).

[18] C.K.Birdsall and A.B.Langdon, *Plasma Physics via Computer Simulation* (McGraw-Hill, New York, 1985).

[19] J.M.Sanz-Serna, Physica D **60**, 293 (1992).

[20] J.deFrutos and J.M.Sanz-Serna, J Comput.Phys **103**, 160 (1992).

Recent Issues of NIFS Series

NIFS-556 H Okumura, S Yamaguchi, H Nakamura, K Ikeda and K Sawada,
Numerical Computation of Thermoelectric and Thermomagnetic Effects, Aug 1998

NIFS-557 Y Takeiri, M. Osakabe, K Tsumori, Y. Oka, O Kaneko, E Asano, T Kawamoto, R Akiyama and M Tanaka,
Development of a High-Current Hydrogen-Negative Ion Source for LHD-NBI System, Aug 1998

NIFS-558 M Tanaka, A Yu Grosberg and T Tanaka,
Molecular Dynamics of Structure Organization of Polyampholytes, Sep. 1998

NIFS-559 R. Horiuchi, K. Nishimura and T Watanabe,
Kinetic Stabilization of Tilt Disruption in Field-Reversed Configurations, Sep 1998
(IAEA-CN-69/THP1/11)

NIFS-560 S. Sudo, K Kholopenkov, K. Matsuoka, S Okamura, C Takahashi, R. Akiyama, A. Fujisawa, K Ida, H Idei, H Iguchi, M Isobe, S Kado, K Kondo, S Kubo, H. Kuramoto, T. Minami, S Morita, S. Nishimura, M Osakabe, M Sasao, B Peterson, K Tanaka, K Toi and Y Yoshimura,
Particle Transport Study with Tracer-Encapsulated Solid Pellet Injection, Oct 1998
(IAEA-CN-69/EXP1/18)

NIFS-561 A. Fujisawa, H. Iguchi, S. Lee, K Tanaka, T Minami, Y Yoshimura, M. Osakabe, K Matsuoka, S. Okamura, H Idei, S Kubo, S Ohdachi, S. Morita, R. Akiyama, K Toi, H. Sanuki, K. Itoh, K Ida, A. Shimizu, S. Takagi, C Takahashi, M. Kojima, S. Hidekuma, S. Nishimura, M. Isobe, A. Ejiri, N. Inoue, R Sakamoto, Y Hamada and M Fujiwara,
Dynamic Behavior Associated with Electric Field Transitions in CHS Heliotron/Torsatron, Oct 1998
(IAEA-CN-69/EX5/1)

NIFS-562 S Yoshikawa,
Next Generation Toroidal Devices; Oct 1998

NIFS-563 Y. Todo and T. Sato,
Kinetic-Magnetohydrodynamic Simulation Study of Fast Ions and Toroidal Alfvén Eigenmodes, Oct 1998
(IAEA-CN-69/THP2/22)

NIFS-564 T. Watari, T. Shimozuma, Y Takeiri, R. Kumazawa, T. Mutoh, M. Sato, O Kaneko, K. Ohkubo, S. Kubo, H. Idei, Y Oka, M Osakabe, T Seki, K. Tsumori, Y Yoshimura, R. Akiyama, T. Kawamoto, S. Kobayashi, F. Shimpo, Y Takita, E Asano, S. Itoh, G Nomura, T. Ido, M Hamabe, M. Fujiwara, A Iiyoshi, S Morimoto, T Bigelow and Y P Zhao,
Steady State Heating Technology Development for LHD; Oct. 1998
(IAEA-CN-69/FTP/21)

NIFS-565 A Sagara, K.Y. Watanabe, K Yamazaki, O. Motojima, M. Fujiwara, O. Mitarai, S Imagawa, H Yamanishi, H. Chikaraishi, A Kohyama, H Matsui, T Muroga, T. Noda, N. Ohyabu, T Satow, A.A Shishkin, S Tanaka, T Terai and T. Uda,
LHD-Type Compact Helical Reactors; Oct 1998
(IAEA-CN-69/FTP/03(R)

NIFS-566 N. Nakajima, J Chen, K. Ichiguchi and M. Okamoto,
Global Mode Analysis of Ideal MHD Modes in L=2 Heliotron/Torsatron Systems; Oct 1998
(IAEA-CN-69/THP1/08)

NIFS-567 K Ida, M. Osakabe, K Tanaka, T. Minami, S. Nishimura, S Okamura, A. Fujisawa, Y. Yoshimura, S Kubo, R Akiyama, D.S.Darrow, H Idei, H. Iguchi, M Isobe, S Kado, T Kondo, S. Lee, K. Matsuoka, S Morita, I Nomura, S. Ohdachi, M Sasao, A Shimizu, K Tumori, S. Takayama, M. Takechi, S Takagi, C. Takahashi, K. Toi and T. Watari,
Transition from L Mode to High Ion Temperature Mode in CHS Heliotron/Torsatron Plasmas, Oct 1998
(IAEA-CN-69/EX2/2)

NIFS-568 S Okamura, K. Matsuoka, R. Akiyama, D.S. Darrow, A. Ejiri, A. Fujisawa, M Fujiwara, M Goto, K. Ida H. Idei, H. Iguchi, N Inoue M. Isobe, K Itoh, S. Kado, K. Khlopenkov, T. Kondo, S Kubo, A Lazaros, S. Lee, G. Matsunaga, T. Minami, S. Morita, S. Murakami, N. Nakajima, N. Nikai, S Nishimura, I Nomura, S. Ohdachi, K. Ohkuni, M. Osakabe, R Pavlichenko, B Peterson, R Sakamoto, H Sanuki, M. Sasao, A. Shimizu, Y. Shirai, S Sudo, S. Takagi, C Takahashi, S Takayama, M Takechi, K Tanaka, K Toi, K. Yamazaki, Y. Yoshimura and T Watari,
Confinement Physics Study in a Small Low-Aspect-Ratio Helical Device CHS Oct 1998
(IAEA-CN-69/OV4/5)

NIFS-569 M.M Skoric, T Sato, A Maluckov, M.S. Jovanovic,
Micro- and Macro-scale Self-organization in a Dissipative Plasma, Oct 1998

NIFS-570 T Hayashi, N Mizuguchi, T-H. Watanabe, T Sato and the Complexity Simulation Group,
Nonlinear Simulations of Internal Reconnection Event in Spherical Tokamak, Oct 1998
(IAEA-CN-69/TH3/3)

NIFS-571 A. Iiyoshi, A. Komori, A. Ejiri, M. Emoto, H. Funaba, M. Goto, K. Ida, H. Idei, S. Inagaki, S. Kado, O. Kaneko, K. Kawahata, S Kubo, R. Kumazawa, S. Masuzaki, T. Minami, J Miyazawa, T. Morisaki, S. Morita, S. Murakami, S. Muto, T. Muto, Y. Nagayama, Y. Nakamura, H. Nakanishi, K. Narihara, K. Nishimura, N. Noda, T. Kobuchi, S. Ohdachi, N. Ohyabu, Y Oka, M. Osakabe, T. Ozaki, B.J. Peterson, A. Sagara, S. Sakakibara, R. Sakamoto, H. Sasao, M. Sasao, K. Sato, M. Sato, T Seki, T. Shimozuma, M. Shoji, H. Suzuki, Y. Takeiri, K. Tanaka, K. Toi, T. Tokuzawa, K. Tsumori, I. Yamada, H. Yamada, S. Yamaguchi, M. Yokoyama, K.Y.Watanabe, T. Watari, R. Akiyama, H. Chikaraishi, K. Haba, S. Hamaguchi, S. Iima, S. Imagawa, N. Inoue, K. Iwamoto, S. Kitagawa, Y. Kubota, J. Kodaira, R. Maekawa, T. Mito. T. Nagasaka, A. Nishimura, Y. Takita, C. Takahashi, K. Takahata, K. Yamauchi, H. Tamura, T. Tsuzuki, S. Yamada, N. Yanagi, H. Yonezu, Y. Hamada, K. Matsuoka, K. Murai, K. Ohkubo, I. Ohtake, M. Okamoto, S. Sato, T. Satow, S. Sudo, S. Tanahashi, K. Yamazaki, M. Fujiwara and O. Motojima,
An Overview of the Large Helical Device Project; Oct. 1998
(IAEA-CN-69/OV1/4)

NIFS-572 M. Fujiwara, H. Yamada, A. Ejiri, M. Emoto, H. Funaba, M. Goto, K. Ida, H. Idei, S. Inagaki, S. Kado, O. Kaneko, K. Kawahata, A. Komori, S. Kubo, R. Kumazawa, S. Masuzaki, T. Minami, J. Miyazawa, T. Morisaki, S. Morita, S. Murakami, S. Muto, T. Muto, Y. Nagayama, Y. Nakamura, H. Nakanishi, K. Narihara, K. Nishimura, N. Noda, T. Kobuchi, S. Ohdachi, N. Ohyabu, Y. Oka, M. Osakabe, T. Ozaki, B. J. Peterson, A. Sagara, S. Sakakibara, R. Sakamoto, H. Sasao, M. Sasao, K. Sato, M. Sato, T. Seki, T. Shimozuma, M. Shoji, H. Sazuki, Y. Takeiri, K. Tanaka, K. Toi, T. Tokuzawa, K. Tsumori, I Yamada, S. Yamaguchi, M. Yokoyama, K.Y Watanabe, T. Watari, R. Akiyama, H. Chikaraishi, K. Haba, S. Hamaguchi, M. Iima, S. Imagawa, N. Inoue, K. Iwamoto, S. Kitagawa, Y. Kubota, J. Kodaira, R. Maekawa, T. Mito, T. Nagasaka, A. Nishimura, Y. Takita, C Takahashi, K. Takahata, K. Yamauchi, H. Tamura, T. Tsuzuki, S Yamada, N. Yanagi, H. Yonezu, Y. Hamada, K. Matsuoka, K. Murai, K. Ohkubo, I. Ohtake, M. Okamoto, S. Sato, T. Satow, S. Sudo, S. Tanahashi, K. Yamazaki, O. Motojima and A. Iiyoshi,
Plasma Confinement Studies in LHD; Oct. 1998
(IAEA-CN-69/EX2/3)

NIFS-573 O. Motojima, K. Akaishi, H. Chikaraishi, H. Funaba, S. Hamaguchi, S. Imagawa, S. Inagaki, N. Inoue, A. Iwamoto, S. Kitagawa, A. Komori, Y. Kubota, R. Maekawa, S. Masuzaki, T. Mito, J. Miyazawa, T. Morisaki, T. Muroga, T. Nagasaka, Y. Nakmura, A. Nishimura, K. Nishimura, N. Noda, N. Ohyabu, S. Sagara, S. Sakakibara, R. Sakamoto, S. Satoh, T. Satow, M. Shoji, H. Suzuki, K. Takahata, H. Tamura, K. Watanabe, H. Yamada, S. Yamada, S. Yamaguchi, K. Yamazaki, N. Yanagi, T. Baba, H. Hayashi, M. Iima, T. Inoue, S. Kato, T. Kato, T. Kondo, S. Moriuchi, H. Ogawa, I. Ohtake, K. Ooba, H. Sekiguchi, N Suzuki, S. Takami, Y. Taniguchi, T Tsuzuki, N. Yamamoto, K. Yasui, H. Yonezu, M. Fujiwara and A. Iiyoshi,
Progress Summary of LHD Engineering Design and Construction; Oct. 1998
(IAEA-CN-69/FT2/1)

NIFS-574 K. Toi, M. Takechi, S. Takagi, G. Matsunaga, M. Isobe, T. Kondo, M. Sasao, D.S. Darrow, K. Ohkuni, S. Ohdachi, R. Akiyama A. Fujisawa, M. Gotoh, H. Idei, K. Ida, H. Iguchi, S. Kado, M. Kojima, S. Kubo, S. Lee, K. Matsuoka, T. Minami, S. Morita, N. Nikai, S. Nishimura, S. Okamura, M. Osakabe, A. Shimizu, Y. Shirai, C. Takahashi, K. Tanaka, T. Watari and Y. Yoshimura,
Global MHD Modes Excited by Energetic Ions in Heliotron/Torsatron Plasmas;Oct. 1998
(IAEA-CN-69/EXP1/19)

NIFS-575 Y. Hamada, A. Nishizawa, Y. Kawasumi, A. Fujisawa, M. Kojima, K. Narihara, K. Ida, A. Ejiri, S. Ohdachi, K. Kawahata, K. Toi, K. Sato, T. Seki, H. Iguchi, K. Adachi, S. Hidekuma, S.Hirokura, K. Iwasaki, T. Ido, R. Kumazawa, H. Kuramoto, T. Minami, I.. Nomura, M. Sasao, K.N. Sato, T. Tsuzuki, I. Yamada and T. Watari,
Potential Turbulence in Tokamak Plasmas;Oct. 1998
(IAEA-CN-69/EXP2/14)

NIFS-576 S. Murakami, U. Gasparino, H. Idei, S. Kubo, H. Maassberg, N. Marushchenko, N. Nakajima, M Romé and M Okamoto.
5D Simulation Study of Suprathermal Electron Transport in Non-Axisymmetric Plasmas;Oct 1998
(IAEA-CN-69/THP1/01)

NIFS-577 S. Fujiwara and T. Sato,
Molecular Dynamics Simulation of Structure Formation of Short Chain Molecules; Nov. 1998

NIFS-578 T. Yamagishi,
Eigenfunctions for Vlasov Equation in Multi-species Plasmas Nov. 1998

NIFS-579 M. Tanaka, A. Yu Grosberg and T. Tanaka,
Molecular Dynamics of Strongly-Coupled Multichain Coulomb Polymers in Pure and Salt Aqueous Solutions;Nov. 1998

NIFS-580 J. Chen, N. Nakajima and M. Okamoto,
Global Mode Analysis of Ideal MHD Modes in a Heliotron/Torsatron System: I. Mercier-unstable Equilibria;Dec. 1998

NIFS-581 M. Tanaka, A. Yu Grosberg and T. Tanaka,
Comparison of Multichain Coulomb Polymers in Isolated and Periodic Systems: Molecular Dynamics Study; Jan. 1999

NIFS-582 V.S. Chan and S. Murakami,
Self-Consistent Electric Field Effect on Electron Transport of ECH Plasmas; Feb. 1999

NIFS-583 M. Yokoyama, N. Nakajima, M. Okamoto, Y. Nakamura and M. Wakatani,

Roles of Bumpy Field on Collisionless Particle Confinement in Helical-Axis Heliotrons, Feb 1999

NIFS-584 T.-H. Watanabe, T. Hayashi, T. Sato, M. Yamada and H. Ji,
Modeling of Magnetic Island Formation in Magnetic Reconnection Experiment, Feb 1999

NIFS-585 R. Kumazawa, T. Mutoh, T. Seki, F. Shinpo, G. Nomura, T. Ido, T. Watari, Jean-Marie Noterdaeme and Yangping Zhao,
Liquid Stub Tuner for Ion Cyclotron Heating; Mar. 1999

NIFS-586 A. Sagara, M. Iima, S. Inagaki, N. Inoue, H. Suzuki, K. Tsuzuki, S. Masuzaki, J. Miyazawa, S. Morita, Y. Nakamura, N. Noda, B. Peterson, S. Sakakibara, T. Shimozuma, H. Yamada, K. Akaishi, H. Chikaraishi, H. Funaba, O. Kaneko, K. Kawahata, A. Komori, N. Ohyabu, O. Motojima, LHD Exp. Group 1, LHD Exp. Group 2,
Wall Conditioning at the Starting Phase of LHD; Mar. 1999

NIFS-587 T. Nakamura and T. Yabe,
Cubic Interpolated Propagation Scheme for Solving the Hyper-Dimensional Vlasov-Poisson Equation in Phase Space, Mar. 1999

NIFS-588 W.X. Wnag, N. Nakajima, S. Murakami and M. Okamoto,
An Accurate δf Method for Neoclassical Transport Calculation, Mar. 1999

NIFS-589 K. Kishida, K. Araki, S. Kishiba and K. Suzuki,
Local or Nonlocal? Orthonormal Divergence-free Wavelet Analysis of Nonlinear Interactions in Turbulence; Mar. 1999

NIFS-590 K. Araki, K. Suzuki, K. Kishida and S. Kishiba,
Multiresolution Approximation of the Vector Fields on T^3; Mar. 1999

NIFS-591 K. Yamazaki, H. Yamada, K.Y. Watanabe, K. Nishimura, S. Yamaguchi, H. Nakanishi, A. Komori, H. Suzuki, T. Mito, H. Chikaraishi, K. Murai, O. Motojima and the LHD Group,
Overview of the Large Helical Device (LHD) Control System and Its First Operation; Apr. 1999

NIFS-592 T. Takahashi and Y. Nakao,
Thermonuclear Reactivity of D-T Fusion Plasma with Spin-Polarized Fuel; Apr. 1999

NIFS-593 H. Sugama,
Damping of Toroidal Ion Temperature Gradient Modes; Apr. 1999

NIFS-594 Xiaodong Li,
Analysis of Crowbar Action of High Voltage DC Power Supply in the LHD ICRF System, Apr. 1999

NIFS-595 K. Nishimura, R. Horiuchi and T. Sato,
Drift-kink Instability Induced by Beam Ions in Field-reversed Configurations; Apr. 1999

NIFS-596 Y. Suzuki, T.-H. Watanabe, T. Sato and T. Hayashi,
Three-dimensional Simulation Study of Compact Toroid Plasmoid Injection into Magnetized Plasmas; Apr. 1999

NIFS-597 H. Sanuki, K. Itoh, M. Yokoyama, A. Fujisawa, K. Ida, S. Toda, S.-I. Itoh, M. Yagi and A. Fukuyama,
Possibility of Internal Transport Barrier Formation and Electric Field Bifurcation in LHD Plasma, May 1999

NIFS-598 S. Nakazawa, N. Nakajima, M. Okamoto and N. Ohyabu,
One Dimensional Simulation on Stability of Detached Plasma in a Tokamak Divertor, June 1999

NIFS-599 S. Murakami, N. Nakajima, M. Okamoto and J. Nhrenberg,
Effect of Energetic Ion Loss on ICRF Heating Efficiency and Energy Confinement Time in Heliotrons, June 1999

NIFS-600 R. Horiuchi and T. Sato,
Three-Dimensional Particle Simulation of Plasma Instabilities and Collisionless Reconnection in a Current Sheet;, June 1999

NIFS-601 W. Wang, M. Okamoto, N. Nakajima and S. Murakami,
Collisional Transport in a Plasma with Steep Gradients; June 1999

NIFS-602 T. Mutoh, R Kumazawa, T. Saki, K. Saito, F. Simpo, G. Nomura, T. Watari, X. Jikang, G Cattanei, H. Okada, K. Ohkubo, M Sato, S. Kubo, T Shimozuma, H. Idei, Y. Yoshimura, O. Kaneko, Y. Takein, M. Osakabe, Y. Oka, K. Tsumori, A. Komori, H Yamada, K. Watanabe, S. Sakakibara, M. Shoji, R. Sakamoto, S. Inagaki, J. Miyazawa, S. Morita, K. Tanaka, B.J. Peterson, S Murakami, T Minami, S. Ohdachi, S. Kado, K. Nanhara, H. Sasao, H. Suzuki, K Kawahata, N. Ohyabu, Y Nakamura, H. Funaba, S. Masuzaki, S. Muto, K. Sato, T. Morisaki, S. Sudo, Y. Nagayama, T. Watanabe, M. Sasao, K.. Ida, N. Noda, K. Yamazaki, K. Akaishi, A. Sagara, K. Nishimura, T. Ozaki, K. Toi, O. Motojima, M. Fujiwara, A. Iiyoshi and LHD Exp. Group 1 and 2,
First ICRF Heating Experiment in the Large Helical Device, July 1999

NIFS-603 P.C. de Vries, Y. Nagayama, K. Kawahata, S. Inagaki, H. Sasao and K. Nagasaki,
Polarization of Electron Cyclotron Emission Spectra in LHD; July 1999

NIFS-604 W. Wang, N. Nakajima, M. Okamoto and S. Murakami,
δf Simulation of Ion Neoclassical Transport; July 1999

NIFS-605 T Hayashi, N Mizuguchi, T. Sato and the Complexity Simulation Group,
Numerical Simulation of Internal Reconnection Event in Spherical Tokamak, July 1999

NIFS-606 M. Okamoto, N. Nakajima and W. Wang,
On the Two Weighting Scheme for δf Collisional Transport Simulation, Aug. 1999

NIFS-607 O. Motojima, A.A. Shishkin, S. Inagaki, K. Y. Watanabe,
Possible Control Scenario of Radial Electric Field by Loss-Cone-Particle Injection into Helical Device. Aug 1999

NIFS-608 R. Tanaka, T. Nakamura and T Yabe,
Constructing Exactly Conservative Scheme in Non-conservative Form; Aug. 1999

NIFS-609 H Sugama,
Gyrokinetic Field Theory; Aug. 1999

NIFS-610 M. Takechi, G. Matsunaga, S. Takagi, K.Ohkuni, K. Toi, M. Osakabe, M. Isobe, S. Okamura, K. Matsuoka, A. Fujisawa, H. Iguchi, S. Lee, T. Minami, K. Tanaka, Y. Yoshimura and CHS Group,
Core Localized Toroidal Alfven Eigenmodes Destabilized By Energetic Ions in the CHS Heliotron/Torsatron; Sep. 1999

NIFS-611 K. Ichiguchi,
MHD Equilibrium and Stability in Heliotron Plasmas; Sep. 1999

NIFS-612 Y. Sato, M. Yokoyama, M. Wakatani and V. D. Pusovitov,
Complete Suppression of Pfirsch-Schluter Current in a Toroidal l=3 Stellarator; Oct. 1999

NIFS-613 S. Wang, H. Sanuki and H. Sugama,
Reduced Drift Kinetic Equation for Neoclassical Transport of Helical Plasmas in Ultra-low Collisionality Regime; Oct. 1999

NIFS-614 J. Miyazawa, H. Yamada, K. Yasui, S. Kato, N., Fukumoto, M. Nagata and T. Uyama,
Design of Spheromak Injector Using Conical Accelerator for Large Helical Device; Nov. 1999

NIFS-615 M. Uchida, A. Fukuyama, K. Itoh, S.-I. Itoh and M. Yagi,
Analysis of Current Diffusive Ballooning Mode in Tokamaks; Dec 1999

NIFS-616 M. Tanaka, A.Yu Grosberg and T. Tanaka,
Condensation and Swelling Behavior of Randomly Charged Multichain Polymers by Molecular Dynamics Simulations; Dec. 1999

NIFS-617 S. Goto and S Kida,
Sparseness of Nonlinear Coupling; Dec. 1999

NIFS-618 M.M. Skoric, T. Sato, A. Maluckov and M.S. Jovanovic,
Complexity in Laser Plasma Instabilities Dec. 1999

NIFS-619 T.-H. Watanabe, H. Sugama and T. Sato,
Non-dissipative Kinetic Simulation and Analytical Solution of Three-mode Equations of Ion Temperature Gradient Instability; Dec. 1999